Journal of Applied Physics

The mechanism of the area negative thermal expansion in $KBe_2BO_3F_2$ family crystals: A first-principles study

Cite as: J. Appl. Phys. **119**, 055901 (2016); https://doi.org/10.1063/1.4941266
Submitted: 02 November 2015 . Accepted: 21 January 2016 . Published Online: 05 February 2016

Xingxing Jiang, Maxim S. Molokeev, Wei Li, Shaofan Wu, Zheshuai Lin, Yicheng Wu, and Chuangtian Chen

The mechanism of the area negative thermal expansion in $KBe_2BO_3F_2$ family crystals: A first-principles study

Xingxing Jiang,[1,2] Maxim S. Molokeev,[3,4] Wei Li,[5] Shaofan Wu,[6] Zheshuai Lin,[1,a)] Yicheng Wu,[1] and Chuangtian Chen[1]

[1]*Center for Crystal Research and Development, Key Lab of Functional Crystals and Laser Technology of Chinese Academy of Sciences, Technical Institute of Physics and Chemistry, Chinese Academy of Sciences, Beijing 100190, China*
[2]*University of Chinese Academy of Sciences, Beijing 100049, China*
[3]*Laboratory of Crystal Physics, Kirensky Institute of Physics, SB RAS, Krasnoyarsk 660036, Russia*
[4]*Department of Physics, Far Eastern State Transport University, Khabarovsk 680021, Russia*
[5]*School of Physics and Wuhan National High Magnetic Field Center, Huazhong University of Science and Technology, Wuhan 430074, China*
[6]*Fujian Institute of Research on the Structure of Matter, Chinese Academy of Sciences, Fuzhou, Fujian 350002, China*

(Received 2 November 2015; accepted 21 January 2016; published online 5 February 2016)

A very recent study demonstrated that the $KBe_2BO_3F_2$ (KBBF) family of crystals, including KBBF, $RbBe_2BO_3F_2$, and $CsBe_2BO_3F_2$, are the only known borates exhibiting a rarely occurring isotropic area negative thermal expansion (NTE) behavior, over a very large temperature range. In the present work, the NTE mechanism in these crystals is comprehensively investigated using the first-principles calculations. It is revealed that the area NTE behavior mainly originates from the concerted distortion of $[BeO_3F]$ tetrahedra in the two-dimensional $[Be_2BO_3F_2]_\infty$ framework with respect to temperature, while the $[BO_3]$ triangles remain almost rigid. Moreover, the different magnitude of NTE effect in the three crystals is attributed to the interaction difference between the alkali metal atoms (K, Rb, or Cs) and the $[Be_2BO_3F_2]_\infty$ layer. © *2016 AIP Publishing LLC*.
[http://dx.doi.org/10.1063/1.4941266]

I. INTRODUCTION

Most materials expand in three-dimensions when subjected to the increasing temperature. However, a small number of materials contract along some specific directions when heated, so are said to exhibit a negative thermal expansion (NTE).[1–7] NTE materials have very important applications, especially, in the high-precision instruments used in temperature-fluctuating environments.[8] The exploration of new NTE materials, therefore, has been one of the research hotspots in the functional materials science and technology since the discovery of this physical effect in the alloy Invar one century ago.[9] To date, NTE has been discovered in a wide range of materials, such as ZrW_2O_8,[1] ScF_3-type materials,[10–12] $PbTiO_3$-based materials,[4–6] antiperovskite materials,[13–15] $LaFe_{13-x}Si_x$ materials,[7] AM_2O_7-type crystals,[16,17] $Sc_2(WO_4)_3$,[18] $NaZr_2(PO_4)_3$-type crystals,[19,20] zeolites,[21] cyanides materials,[22–24] and metal organic frameworks.[25,26] Several models have been proposed to rationalize NTE in these materials, e.g., rigid unit model (RUM),[1,27] spontaneous volume ferroelectrostriction,[4] ferromagnetic-to-paramagnetic phase transition,[7] geometrically flexible diatomic linkages mechanism,[2,28] and transverse vibration of bridging oxygen mechanism.[29] These models not only provide an in-depth sight to this rarely occurring thermal behavior but also give a very useful guidance to the exploration of new NTE materials.

In a crystal, the NTE behavior can be manifested in one-dimension (linear), in two-dimensions (in area), or in three-dimensions (in volume), and the microscopic mechanisms would be some what different from one type to another. For instance, the giant linear NTE effect in $Ag_3[Co(CN)_6]$ originates from its flexing fence-like framework,[2] and the area NTE behaviors in $Ni(CN)_2$,[30] NaV_2O_5,[31] and graphene[32] are attributed to "Lifshitz mechanism" of rapid interlayer expansion coupled with contraction in the perpendicular directions with increasing temperature. For the volume NTE behaviors, the intrinsic mechanisms are usually due to the strengthening of the transverse vibrations between the rigid groups or the phase-transition processes,[4] such as the "rigid unit model" in ZrW_2O_8,[27] ferroelectric phase transition in $PbTiO_3$-based materials,[6] and ferromagnetic-to-paramagnetic phase transition in $LaFe_{13-x}Si_x$ materials.[7]

Recently, the explorations of NTE materials have been focused on the borate system. It is well known that a boron atom can be three- or four-fold coordinated with oxygen atoms, forming a BO_3 triangle or BO_4 tetrahedron, and their spatial combinations result in the large structural diversity in borates.[33,34] This implies that this system would possess many interesting physical properties because of the paradigm "structure determines property." In fact, quite a few borate crystals have been reported to exhibit the NTE behaviors such as the nonlinear optical crystal BiB_3O_6 and LiB_3O_5, whose NTE behaviors are attributed to the rotation of the rigid borate units.[35,36] However, these studies just concentrated on the influence of thermal expansion anisotropy on the single crystal growth of borates which usually adopts the

a)Author to whom correspondence should be addressed. Electronic mail: zslin@mail.ipc.ac.cn.

high-temperature melt method, and their NTE phenomena only occur along one direction (i.e., in one-dimensional, 1D).[37,38] From application perspective, the isotropic NTE effects in higher dimension (2D or even 3D) are much more useful.

Recently, the area NTE behaviors were discovered in two borates: $LiBeBO_3$[39] and $KZnB_3O_6$.[40] The area NTE effects in both compounds are resulted from the interaction between the rotation of rigid borate units and anharmonic vibration of alkali ions.[39,40] However, their area NTE behaviors are not isotropic. Very recently, we have further identified an isotropic area NTE effect in the $KBe_2BO_3F_2$ (KBBF) family crystals.[41] The KBBF family crystals consist of KBBF, $RbBe_2BO_3F_2$ (RBBF), and $CsBe_2BO_3F_2$ (CBBF). All these three crystals exhibit the NTE behavior over very large temperature range from 48 K to 848 K, with the area thermal expansion coefficients of $-9.2(1)$ m K^{-1}, $-11.0(1)$ m K^{-1}, and $-15.1(2)$ m K^{-1} in the *ab* plane for KBBF, RBBF, and CBBF, respectively.[41] The KBBF family crystals are the only known isotropic area NTE borates, which would have a unique role to link the 1D and 3D NTE effects in borates. However, the NTE mechanism in these crystals has not been systematically investigated yet. In this work, using the first-principles calculations, we investigate the relationship between structure and property for the area NTE effects in the KBBF family crystals. Furthermore, the role of alkali atoms (K, Rb, or Cs) to adjust the magnitude of NTE behavior is discussed.

II. COMPUTATIONAL METHODS

Normally, the variable temperature X-ray diffraction has been considered to be a routine experimental method to investigate the variation of atomic structures with respect to the temperature fluctuation. However, since the NTE behavior is rather weak in the KBBF family crystals (despite over large temperature range), quite a few factors, such as the background (particularly at high angles) and strong preferred orientation due to its layered structural feature (e.g., (001) peak), would heavily deteriorate the accurate determination of the detailed structural modifications. In addition, in order to fully understand the NTE mechanism, it is very crucial to determine the precise atomic position of Be atoms. But this is very hard because Be is among the lightest elements with only 4 electrons each: most of the diffraction intensity is concentrated on the alkali atoms (K, Rb, or Cs) in the studied crystals. Owing to the limitation of variable temperature X-ray diffraction experiments, the state-of-the-art first-principles method becomes a powerful and precise tool to elucidate the underlying structural mechanism of NTE. In fact, for the KBBF family crystals, the optical and mechanical properties (which are very sensitive to the detailed atomic positions) have been accurately determined by the first-principles calculations.[41,42] The good agreement between calculated and experimental results clearly demonstrates the reliability and validity of the computational methods adopted in this work.

The first-principles calculations were performed by CASTEP,[43] a total energy package based on plane-wave pseudopotential density functional theory (DFT).[44,45] The functionals developed by Ceperley, Alder, Perdew, and Zunger (CA-PZ)[46,47] in local density approximation (LDA) form were adopted to search the minimal of the total energy. The effective interaction between atoms cores and valence electrons were modeled by optimized norm-conserving pseudopotentials[48] in Kleinman–Bylander form,[49] which allow us to adopt a relatively small basis set without compromising the computational accuracy. The K $3s^2 3p^6 4s^1$, Rb $4s^2 4p^6 5s^1$, Cs $5s^2 5p^6 6s^1$, Be $2s^2$, B $2s^2 2p^1$, O $2s^2 2p^4$, and F $2s^2 2p^5$ electrons were treated as valence electrons. A very high kinetic energy cutoff of 900 eV and dense Monkhorst–Pack[50] $4 \times 4 \times 2$k-point meshes in the Brillouin zones were chosen. The Broyden–Fletcher–Goldfarb–Shanno (BFGS)[51] minimization scheme was employed in the geometry optimization and the convergence criteria were set to 5.0×10^{-5} eV/atom, 0.1 eV/Å, 0.2 GPa, and 5.0×10^{-3} Å for energy, maximum force, maximum stress and maximum displacement, respectively. The tests about functionals and k-point (see Tables S1 and S2 in the supplementary material[52]) in KBBF revealed that the above computational parameters are sufficiently accurate for the purpose of this study. To account for the deviation of the calculated and experimental cell parameters, in the geometry optimizations, the cell parameters were fixed at the experimental values[41] (listed in Table S3[52]). Based on the optimized crystal structures, the atomic vibrational (phonon) properties were calculated by linear response formalism,[53] in which the phonon frequencies were obtained by the second derivative of the total energy with respect to a finite perturbation. The quasiharmonic approximation method based on DFT method has been maturely used to predict thermal expansion behavior of materials.[27,54] Since the NTE behavior of KBBF family has been experimentally determined, the method adopted in this work is feasible to study their NTE mechanism and has been successfully applied to investigate the NTE effects in borates.[39] It should be emphasized that the methodology adopted in the present work actually gives almost the same physical insight as the Grüneisen parameters calculations on the vibration modes (see Table S4[52]).

III. RESULTS AND DISCUSSION

The KBBF family crystals, KBBF, RBBF, and CBBF, possess almost the same crystal structures: the crystals are composed of 2D infinite $[Be_2BO_3F_2]_\infty$ layers along the *ab* plane, while the alkali atoms (K, Rb, or Cs) reside between the layers *via* relatively weak electrostatic interactions (Fig. 1(a)). The $[Be_2BO_3F_2]_\infty$ layer is constructed by $[BO_3]$ triangles and $[BeO_3F]$ tetrahedra, which are alternatively distributed by sharing the corner oxygen atoms in the ratio 2:1 (Fig. 1(b)). The overall geometries of the $[Be_2BO_3F_2]_\infty$ layer are almost identical for KBBF, RBBF, and CBBF. All three crystals crystallize in the hexagonal space group *R*32, and the uniaxial symmetry ensures the KBBF family crystals exhibiting the isotropic physical properties in the *ab* plane according to Neumann's principle.[55]

Fig. 2 displays the variation of the calculated bond lengths and angles in KBBF, RBBF, and CBBF under different temperatures (the values are also listed in Table S5[52]). Clearly, the geometries of 2D infinite $[Be_2BO_3F_2]_\infty$ layers undergo unusual changes in all three crystals as temperature

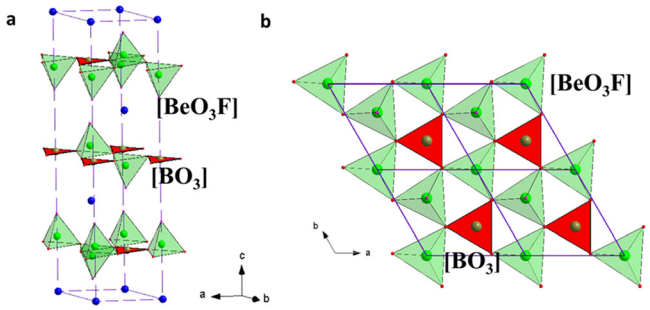

FIG. 1. Crystal structure of KBBF family crystals: (a) Unit cell for the KBBF family crystals. (b) Two-dimensional $(Be_2BO_3F_2)_\infty$ layer. The alkaline (K, Rb, and Cs), boron, beryllium, oxygen, and fluorine atoms are represented by blue, olive, green, red, and pink balls, respectively. The $(BO_3)^{3-}$ and $(BeO_3F)^{5-}$ groups are represented by red triangles and green tetrahedra, respectively.

varies. When the temperature increases from 48 K to 848 K, in the $[BeO_3F]$ tetrahedra the Be-F bond lengths increase from 1.493 Å to 1.502 Å, from 1.447 Å to 1.507 Å, and from 1.505 Å to 1.512 Å (increased by 0.6%, 0.7%, and 0.5%) in KBBF, RBBF, and CBBF, respectively, as shown in Figs. 2(a), 2(d), and 2(g). This observation is in accordance with the common sense that a chemical bond would be elongated as temperature increases. However, under the same temperature range, the Be-O bond lengths contract as the function of temperature and decrease from 1.628 Å to 1.622 Å, from 1.633 Å to 1.627 Å, and from 1.640 Å to 1.630 Å (decreased by 0.4%, 0.4%, and 0.6%) in KBBF, RBBF, and CBBF, respectively (see Figs. 2(a), 2(d), and 2(g)). At the same time, the ∠F-Be-O angles increase gradually from 108.541° to 108.801°, from 108.239° to 108.562°, and from 107.867°

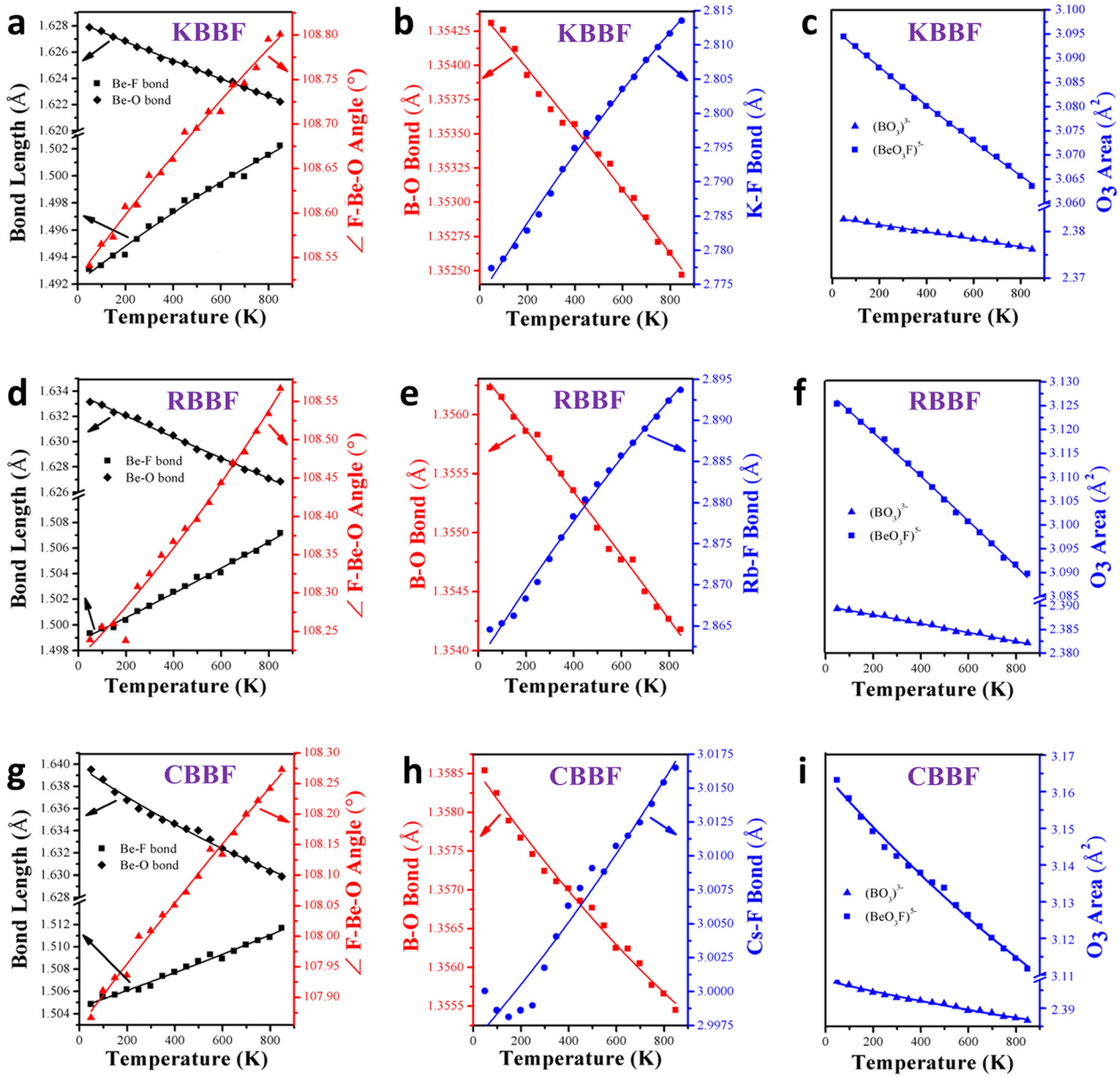

FIG. 2. Variation of atomic structures with respect to the temperature fluctuation: variation of Be-O bond lengths, Be-F bond lengths, and ∠F-Be-O angles in (a) KBBF, (d) RBBF, and (c) CBBF; variation of B-O bond lengths and alkali-fluorine bond lengths in (b) KBBF, (e) RBBF, and (h) CBBF; and variation of the area of O_3 triangles in $(BO_3)^{3-}$ triangles and $(BeO_3F)^{5-}$ tetrahedra in (c) KBBF, (f) RBBF, and (i) CBBF. The points are the first-principles values and the lines are fitted by polynomial fitting method.

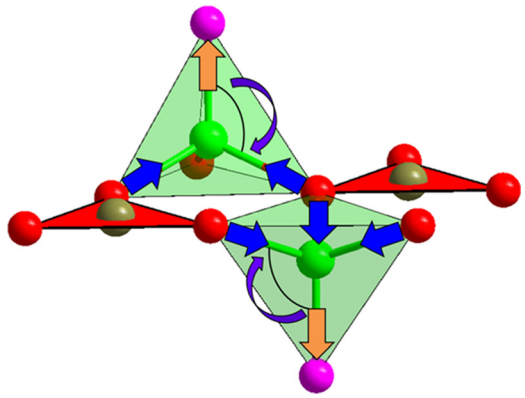

FIG. 3. Schematic for the NTE mechanism in the KBBF family crystals. The orange, blue, and purple arrows represent the elongation of Be-F bonds, contraction of Be-O bonds, and opening of ∠F-Be-O angles with increasing temperature, respectively. [BO_3] and [BeO_3F] groups are represented by red triangles and tetrahedra, respectively.

to 108.273° (increased by 0.2%, 0.3%, and 0.4%) in KBBF, RBBF, and CBBF, respectively (see Figs. 2(a), 2(d), and 2(g)). Both the decrease of Be-O bond lengths and the increase of ∠F-Be-O angles lead to the contraction of the O_3 triangular bases of the [BeO_3F] tetrahedra (see Figs. 2(c), 2(f), and 2(i)), thus contribute to the negative thermal expansion of the $[Be_2BO_3F_2]_\infty$ layers.

Compared with the [BeO_3F] tetrahedra, the [BO_3] triangles in the $[Be_2BO_3F_2]_\infty$ layers are much more rigid because of the strongly covalent interaction between boron and oxygen atoms:[38] from 48 K to 848 K, the B-O bond only decreases from 1.354 Å to 1.352 Å, from 1.356 Å to 1.354 Å, and from 1.359 Å to 1.356 Å (decreased by 0.1%, 0.1%, and 0.2%) in KBBF, RBBF, and CBBF, respectively (see Figs. 2(b), 2(e), and 2(h)). Therefore, the contribution from the distortion of [BO_3] triangles to the NTE effect is much smaller than that from the [BeO_3F] tetrahedra: even if the [BO_3] triangles keep constant during the heating process, the contraction of the O_3 bases in [BeO_3F] tetrahedra still accounts for the 85%, 92%, and 88% of the NTE effects in KBBF, RBBF, and CBBF, respectively (also see Figs. 2(c), 2(f), and 2(i)). This indicates that the NTE behavior in KBBF family crystals mainly originates from the unusual change of [BeO_3F] tetrahedra, i.e., the contraction of Be-O bonds and the opening of ∠F-Be-O angles with respect to the increasing temperature (as depicted in Fig. 3). Interestingly, the crystal structures of the KBBF family crystals are very similar to that of NaV_2O_5,[31] thus they may have the analogous mechanism for the area NTE behaviors.

It is well known that when being heated, the binding interaction between atoms would become weaker and the effective bond lengths would be elongated.[39] Thus, in normal condition, the frequencies of lattice vibrations (i.e., phonon modes) would shift to lower wavenumbers at higher temperature.[56] However, in the NTE effect, certain interatomic distances are abnormally contracted with the increase of temperature, and the corresponding phonon modes would shift to the higher wavenumbers (i.e., phonon mode hardening). Therefore, the identification of the phonon modes which are hardened with the increasing temperature is an alternative way to investigate the NTE mechanism in crystals.

The dominant role of the concerted distortion of [BeO_3F] tetrahedra in NTE behavior is also confirmed by the phonon analysis. A primitive unit cell of KBBF family crystals contains nine atoms, resulting in 27 degrees of freedom at the Γ-point in the Brillouin zone. The irreducible representation of *R*32 space group at Γ-point yields a sum of $18E + 3A_1 + 6A_2$, in which two acoustic modes belong to the E and one belongs to the A_2 irreducible representation: they are independent of the thermal expansion effect and not considered here. Table I lists the calculated phonon frequencies at 48 K and 848 K, as well as the corresponding changes of the phonon modes. Clearly, totally 12 phonon modes are hardened with increasing temperature, indicating that the variation of corresponding interatomic interactions contributes to the NTE effect. The further analysis, as shown in Fig. 4, reveals that these NTE phonon modes are mainly attributed to the stretch and twist of the Be-O and Be-F bonds which results in the distortion of the [BeO_3F] tetrahedra. As a comparison, in the low frequency NTE modes, the [BO_3] triangles almost keep its rigid configuration, and the only NTE modes related to the distortion of [BO_3] groups occur at the highest frequency modes (modes 23 and 24). This demonstrates that the contraction of B-O bonds contributes to the thermal contraction only at very high temperature. Thus, the NTE behavior in the KBBF family crystals dominantly originates from the abnormal distortion of the [BeO_3F] tetrahedra with increasing temperature. In addition, the highest NTE phonon frequencies (modes 23 and 24) are located at 1292.07, 1284.33, and 1275.85 cm^{-1}, corresponding to the temperature of 1861 K, 1850 K, and 1838 K, for KBBF, RBBF, and CBBF, respectively, which implies that the NTE effects in these crystals would occur until very high temperatures.

On the other hand, compared with the modification of $[Be_2BO_3F_2]_\infty$ layers, the variation of interlayer spacings (which can also be measured by the change of alkali and fluorine bond lengths) with temperature fluctuation is more prominent. The K-F, Rb-F, and Cs-F bonds increase from 2.777 Å to 2.814 Å, from 2.865 Å to 2.894 Å, and from 3.000 Å to 3.017 Å (by 1.3%, 1.0%, and 0.6%), respectively, from 48 K to 848 K (Figs. 2(b), 2(e), and 2(h)). The large variation of bond lengths between alkali and fluorine atoms is mainly attributed to the much weaker interaction between these atoms compared with the atomic interaction inside the $[Be_2BO_3F_2]_\infty$ layers. Therefore, the large positive thermal expansion occurs along the *c*-axis in the crystals as temperature increases (51.1 m K^{-1}, 39.6 m K^{-1}, and 25.7 m K^{-1} for KBBF, RBBF, and CBBF, respectively[41]).

Although the $[Be_2BO_3F_2]_\infty$ layers are almost the same in KBBF, RBBF, and CBBF, the NTE effect values in the three crystals are some different: the area NTE coefficients in the *ab* plane are −9.2 m K^{-1}, −11.0 m K^{-1}, and −15.1 m K^{-1} in KBBF, RBBF, and CBBF, respectively.[41] The NTE magnitude difference can be attributed to the different interlayer interaction between the $[Be_2BO_3F_2]_\infty$ layers, which intrinsically depends on the binding interaction between the intercalated alkali atoms and the intralayer fluorine atoms. It is known that, with the increase of atomic radius, the alkali atoms K, Rb, and Cs would have increased chemical bonds

TABLE I. First-principles phonon mode frequencies and their variation at the temperatures 48 K and 848 K.

		KBBF (unit: cm^{-1})			RBBF (unit: cm^{-1})			CBBF (unit: cm^{-1})		
Mode No.	Irre. rep.	48 K	848 K	$\Delta\omega$	48 K	848 K	$\Delta\omega$	48 K	848 K	$\Delta\omega$
1	E	75.23	60.96	−14.27	67.51	59.82	−7.69	63.50	59.57	−3.93
2	E	75.23	60.96	−14.27	67.51	59.82	−7.69	63.50	59.57	−3.93
3	A2	88.01	80.27	−7.74	72.07	67.08	−4.99	69.26	66.77	−2.48
4	E	129.47	124.77	−4.70	137.64	133.67	−3.97	141.99	138.41	−3.58
5	E	129.47	124.77	−4.70	137.64	133.67	−3.97	141.99	138.41	−3.58
6	E	199.68	195.22	−4.47	203.27	199.33	−3.93	203.91	201.08	−2.83
7	E	199.68	195.22	−4.47	203.27	199.33	−3.93	203.91	201.08	−2.83
8	A1	333.75	333.83	0.08	333.54	333.71	0.17	334.19	334.63	0.44
9	E	362.21	358.97	−3.24	362.12	359.02	−3.10	362.00	359.17	−2.83
10	E	362.21	358.97	−3.24	362.12	359.02	−3.10	362.00	359.17	−2.83
11	A2	392.06	392.07	0.01	389.68	389.91	0.23	387.56	388.76	1.20
12	A2	539.14	543.47	4.34	533.72	538.67	4.94	527.24	535.44	8.20
13	E	623.97	631.28	7.31	617.29	626.17	8.88	607.66	622.20	14.54
14	E	623.97	631.28	7.31	617.29	626.17	8.88	607.66	622.20	14.54
15	E	679.71	691.63	11.92	669.45	682.49	13.04	656.80	676.08	19.28
16	E	679.71	691.63	11.92	669.45	682.49	13.04	656.80	676.08	19.28
17	E	703.94	712.19	8.26	696.88	705.27	8.39	689.16	700.69	11.53
18	E	703.94	712.19	8.26	696.88	705.27	8.39	689.16	700.69	11.53
19	A2	716.80	713.58	−3.21	715.22	711.63	−3.59	713.17	709.39	−3.78
20	A2	847.47	837.15	−10.32	835.96	827.19	−8.77	825.47	819.40	−6.07
21	A1	884.29	869.25	−15.04	870.10	856.99	−13.10	855.99	846.02	−9.97
22	A1	922.25	926.02	3.77	915.64	920.48	4.83	908.91	916.73	7.82
23	E	1292.07	1299.29	7.22	1284.33	1292.12	7.79	1275.85	1287.33	11.49
24	E	1292.07	1299.29	7.22	1284.33	1292.12	7.79	1275.85	1287.33	11.49

with fluorine atoms (the calculated binding energies are 0.99 eV, 1.01 eV, and 1.04 eV for K-F, Rb-F, and Cs-F bonds, respectively[41]). This means that the "rigidity" of K-F, Rb-F, and Cs-F bonds would increase when subjected to the thermal perturbation. So, the stretching of alkali-fluorine bonds becomes more and more difficult: from 48 K to 848 K the K-F, Rb-F, and Cs-F expand by 1.3%, 1.0%, and 0.6% (see Figs. 2(b), 2(e), and 2(h)), respectively. Thus, the positive thermal expansion along the *c*-axes exhibits a decreasing tendency from KBBF, RBBF to CBBF (from 51.1 m K^{-1}, 39.6 m K^{-1} to 25.7 m K^{-1}). The increasing alkali-fluorine bond interaction from K-F, Rb-F to Cs-F, on the other hand, leads to the vertex F atoms more and more stretched from the $[BeO_3F]$ tetrahedra with the ∠F-Be-O angles opening of 0.26°, 0.32°, and 0.41° in KBBF, RBBF, and CBBF, respectively, from 48 K to 848 K (see Fig. 5(a)). The larger elongation of $[BeO_3F]$ tetrahedra along the *c*-axis actually leads to the more contraction of these tetrahedra in the *ab* plane, hence the $[Be_2BO_3F_2]_\infty$ layers exhibit more dominant NTE behaviors from KBBF, RBBF to CBBF. Therefore, although the alkali atoms do not directly determine the NTE behaviors, they adjust the NTE magnitude by manipulating their interaction with the $[Be_2BO_3F_2]_\infty$ layers.

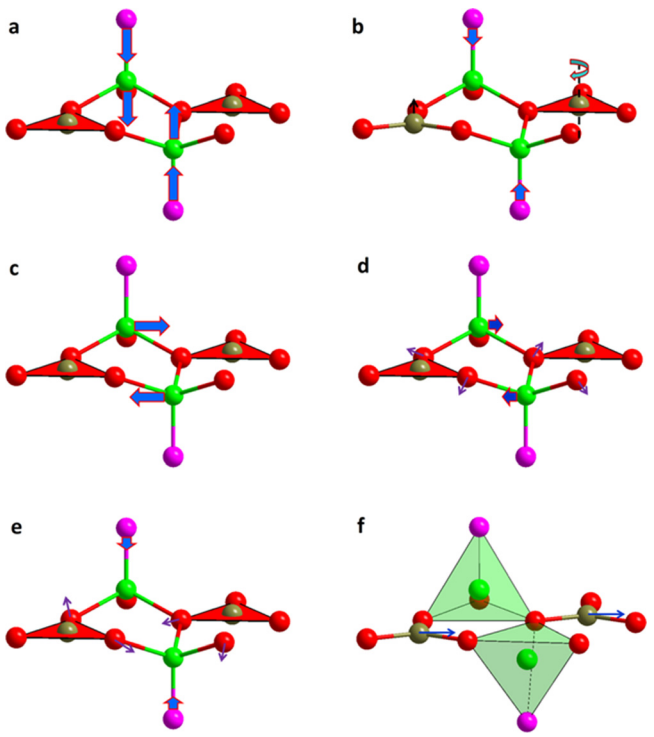

FIG. 4. Atomic vibrations assigned to the NTE phonon modes. (a) Mode 8, (b) Modes 11 and 12, (c) Modes 13, 14, 15, and 16, (d) Modes 17, 18, and 22, and (f) Modes 23 and 24.

The interaction between alkali and fluorine atoms can also influence the atomic vibration property, and the degree of hardening (i.e., the increasing magnitude) of the NTE phonon modes increases from KBBF, RBBF to CBBF (see Fig. 5(b)). Since all NTE phonon modes occur in the $[Be_2BO_3F_2]_\infty$ layers, the increased degree of hardening can be attributed to the enhanced atomic binding interaction in the $[Be_2BO_3F_2]_\infty$ layers from KBBF, RBBF to CBBF with increasing temperature. This, in turn, depends on the alkali-fluorine interaction, because the geometries of $[Be_2BO_3F_2]_\infty$ layers are almost the same in the three crystals.

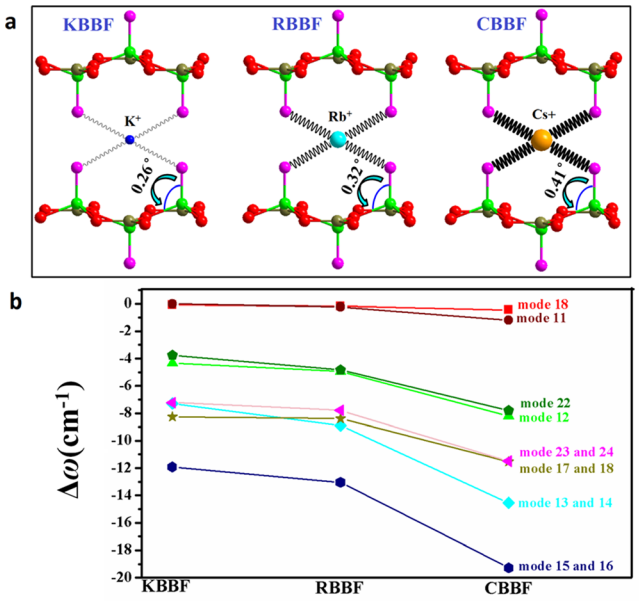

FIG. 5. The mechanism for the enhanced area NTE behavior from KBBF, RBBF to CBBF: (a) schematic for the effect of the bonds between alkali and fluorine atoms with the opening degree of ∠F-Be-O angles and (b) distributions of frequencies change in the NTE phonon modes from 48 K to 848 K in KBBF, RBBF, and CBBF.

IV. CONCLUSIONS

The microscopic mechanism of area NTE effect in the KBBF family crystals was investigated by the first-principles calculations. The geometry optimizations revealed that the NTE behavior in these crystals mainly originates from the distortion of $[BeO_3F]$ tetrahedra in the $[Be_2BO_3F_2]_\infty$ layers. Namely, in the $[BeO_3F]$ tetrahedra, the abnormal contraction of Be-O bonds and opening of the ∠F-Be-O angles with the increasing temperature determine the NTE behavior. As a comparison, the $[BO_3]$ triangles remain almost rigid as temperature fluctuates, and its contribution to the NTE behavior is neglectably small. The further atomic vibration analysis demonstrated that the NTE phonon modes occur in the $[Be_2BO_3F_2]_\infty$ layers and they almost all correspond to the stretch and twist of the $[BeO_3F]$ tetrahedra. On the other hand, although the alkali atoms (K, Rb, Cs) do not determine the NTE behavior, they can significantly affect the magnitude of the NTE effect by their interaction to the $[Be_2BO_3F_2]_\infty$ layers. We believe that the elucidation of the NTE mechanism in the KBBF family crystals has great implication to the further exploration of NTE materials, especially in 2D or 3D, in borates.

ACKNOWLEDGMENTS

This work was supported by the National Scientific Foundations of China (Grant No. 11474292), the Special Foundation of the Director of Technical Institute of Physics and Chemistry (TIPC), and the Opening Project of the Key Laboratory of Cryogenics in TIPC, Chinese Academy of Sciences, China "863" Project (No. 2015AA034203) and "973" Project (No. 2014CB921301).

[1]T. A. Mary, J. S. O. Evans, T. Vogt, and A. W. Sleight, Science **272**, 90 (1996).
[2]A. L. Goodwin, M. Calleja, M. J. Conterio, M. T. Dove, J. S. O. Evans, D. A. Keen, L. Peters, and M. G. Tucker, Science **319**, 794 (2008).
[3]P. Mohn, Nature **400**, 18 (1999).
[4]J. Chen, K. Nittala, J. S. Forrester, J. L. Jones, J. Deng, R. Yu, and X. Xing, J. Am. Chem. Soc. **133**, 11114 (2011).
[5]J. Chen, L. Fan, Y. Ren, Z. Pan, J. Deng, R. Yu, and X. Xing, Phys. Rev. Lett. **110**, 115901 (2013).
[6]J. Chen, L. Hu, J. Deng, and X. Xing, Chem. Soc. Rev. **44**, 3522 (2015).
[7]R. Huang, Y. Liu, W. Fan, J. Tan, F. Xiao, L. Qian, and L. Li, J. Am. Chem. Soc. **135**, 11469 (2013).
[8]P. Lommens, C. De Meyer, E. Bruneel, K. De Buysser, I. Van Driessche, and S. Hoste, J. Eur. Ceram. Soc. **25**, 3605 (2005).
[9]J. R. Davis, *Alloying: Understanding the Basics* (ASM International, 2001).
[10]B. K. Greve, K. L. Martin, P. L. Lee, P. J. Chupas, K. W. Chapman, and A. P. Wilkinson, J. Am. Chem. Soc. **132**, 15496 (2010).
[11]L. Hu, J. Chen, L. Fan, Y. Ren, Y. Rong, Z. Pan, J. Deng, R. Yu, and X. Xing, J. Am. Chem. Soc. **136**, 13566 (2014).
[12]J. C. Hancock, K. W. Chapman, G. J. Halder, C. R. Morelock, B. S. Kaplan, L. C. Gallington, A. Bongiorno, C. Han, S. Zhou, and A. P. Wilkinson, Chem. Mater. **27**, 3912 (2015).
[13]K. Takenaka and H. Takagi, Appl. Phys. Lett. **87**, 261902 (2005).
[14]R. Huang, L. Li, F. Cai, X. Xu, and L. Qian, Appl. Phys. Lett. **93**, 081902 (2008).
[15]C. Wang, L. Chu, Q. Yao, Y. Sun, M. Wu, L. Ding, J. Yan, Y. Na, W. Tang, G. Li, Q. Huang, and J. W. Lynn, Phys. Rev. B **85**, 220103 (2012).
[16]J. S. O. Evans, J. Chem. Soc., Dalton Trans. **1999**, 3317.
[17]Y. Yamamura, A. Horikoshi, S. Yasuzuka, H. Saitoh, and K. Saito, Dalton Trans. **40**, 2242 (2011).
[18]J. S. O. Evans, T. A. Mary, and A. W. Sleight, J. Solid State Chem. **137**, 148 (1998).
[19]K. Kamali, T. R. Ravindran, C. Ravi, Y. Sorb, N. Subramanian, and A. K. Arora, Phys. Rev. B **86**, 144301 (2012).
[20]D. A. Woodcock, P. Lightfoot, and C. Ritter, Chem. Commun. **1998**, 107.
[21]P. Lightfoot, D. A. Woodcock, M. J. Maple, L. A. Villaescusa, and P. A. Wright, J. Mater. Chem. **11**, 212 (2001).
[22]S. Margadonna, K. Prassides, and A. N. Fitch, J. Am. Chem. Soc. **126**, 15390 (2004).
[23]A. L. Goodwin, D. A. Keen, and M. G. Tucker, Proc. Natl. Acad. Sci. U. S. A. **105**, 18708 (2008).
[24]D. J. Williams, D. E. Partin, F. J. Lincoln, J. Kouvetakis, and M. O'Keeffe, J. Solid State Chem. **134**, 164 (1997).
[25]W. Miller, D. S. Mackenzie, C. W. Smith, and K. E. Evans, Mech. Mater. **40**, 351 (2008).
[26]D. Dubbeldam, K. S. Walton, D. E. Ellis, and R. Q. Snurr, Angew. Chem., Int. Ed. **46**, 4496 (2007).
[27]V. Gava, A. L. Martinotto, and C. A. Perottoni, Phys. Rev. Lett. **109**, 195503 (2012).
[28]A. L. Goodwin, Phys. Rev. B **74**, 134302 (2006).
[29]J. S. O. Evans, T. A. Mary, and A. W. Sleight, J. Solid State Chem. **133**, 580 (1997).
[30]T. Matsuda, J. E. Kim, K. Ohoyama, and Y. Moritomo, Phys. Rev. B **79**, 172302 (2009).
[31]M. Koppen, D. Pankert, R. Hauptmann, M. Lang, M. Weiden, C. Geibel, and F. Steglich, Phys. Rev. B **57**, 8466 (1998).
[32]M. Y. Seyidov and R. A. Suleymanov, J. Appl. Phys. **108**, 063540 (2010).
[33]C. T. Chen, N. Ye, J. Lin, J. Jiang, W. R. Zeng, and B. C. Wu, Adv. Mater. **11**, 1071 (1999).
[34]C. T. Chen, T. Sasaki, R. K. Li, Y. C. Wu, Z. S. Lin, Y. Mori, Z. G. Hu, J. Y. Wang, S. Uda, M. Yoshimura, and Y. Kaneda, *Nonlinear Optical Borate Crystals-Principles and Applications* (Wiley-VCH, New York, 2012).
[35]P. Becker and L. Bohaty, Cryst. Res. Technol. **36**, 1175 (2001).
[36]L. Wei, G. Q. Dai, Q. Z. Huang, Z. An, and D. K. Liang, J. Phys. D: Appl. Phys. **23**, 1073 (1990).
[37]R. S. Bubnova and S. K. Filatov, Phys. Status Solidi B **245**, 2469 (2008).
[38]R. S. Bubnova and S. K. Filatov, Z. Kristallogr. **228**, 395 (2013).
[39]W. Yao, X. Jiang, R. Huang, W. Li, C. Huang, Z. Lin, L. Li, and C. Chen, Chem. Commun. **50**, 13499 (2014).
[40]Y. Lou, D. Li, Z. Li, S. Jin, and X. Chen, Sci. Rep. **5**, 10996 (2015).
[41]X. Jiang, S. Luo, L. Kang, P. Gong, W. Yao, H. Huang, W. Li, R. Huang, W. Wang, Y. Li, X. Li, X. Wu, P. Lu, L. Li, C. Chen, and Z. Lin, Adv. Mater. **27**, 4851 (2015).

[42]Z. S. Lin, X. X. Jiang, L. Kang, P. F. Gong, S. Y. Luo, and M. H. Lee, J. Phys. D: Appl. Phys. **47**, 253001 (2014).
[43]S. J. Clark, M. D. Segall, C. J. Pickard, P. J. Hasnip, M. J. Probert, K. Refson, and M. C. Payne, Z. Kristallogr. **220**, 567 (2005).
[44]W. Kohn and L. J. Sham, Phys. Rev. **140**, A1133 (1965).
[45]M. C. Payne, M. P. Teter, D. C. Allan, T. A. Arias, and J. D. Joannopoulos, Rev. Mod. Phys. **64**, 1045 (1992).
[46]D. M. Ceperley and B. J. Alder, Phys. Rev. Lett. **45**, 566 (1980).
[47]J. P. Perdew and A. Zunger, Phys. Rev. B **23**, 5048 (1981).
[48]A. M. Rappe, K. M. Rabe, E. Kaxiras, and J. D. Joannopoulos, Phys. Rev. B **41**, 1227 (1990).
[49]L. Kleinman and D. M. Bylander, Phys. Rev. Lett. **48**, 1425 (1982).
[50]H. J. Monkhorst and J. D. Pack, Phys. Rev. B **13**, 5188 (1976).
[51]B. G. Pfrommer, M. Cote, S. G. Louie, and M. L. Cohen, J. Comput. Phys. **131**, 233 (1997).
[52]See supplementary material at http://dx.doi.org/10.1063/1.4941266 for the test about the computational method, the input cell parameters, and the output bond length and angles.
[53]S. Baroni, S. de Gironcoli, A. Dal Corso, and P. Giannozzi, Rev. Mod. Phys. **73**, 515 (2001).
[54]F. Wang, Y. Xie, J. Chen, H. Fu, and X. Xing, Appl. Phys. Lett. **103**, 221901 (2013).
[55]J. F. Nye, *Physical Properties of Crystals* (Oxford University Press, Oxford, 1957).
[56]G. D. Barrera, J. A. O. Bruno, T. H. K. Barron, and N. L. Allan, J. Phys.: Condens. Matter **17**, R217 (2005).